PNAS
www.pnas.org

Supplementary Information for

Optical dipole-induced anisotropic growth of semiconductors: A facile strategy toward chiral and complex nanostructures

Xiaolin Lu, Xujie Wang, Yong Liu and Tao Ding*
Key Laboratory of Artificial Micro/Nano Structure of Ministry of Education, School of Physics and Technology, Wuhan University, Wuhan, 430072, China.

*Tao Ding.
Email: t.ding@whu.edu.cn

This PDF file includes:

Supplementary Information Text

Supplementary Note 1: photochemistry of K_2PtCl_4 solution

It is known that photoaquation can normally happen to $[PtCl_4]^{2-}$ complexes, which form the $[PtCl_3(H_2O)]^{2-}$ hydrates and $Cl^{\cdot}$ radicals (S1). The latter can further oxide the Pt(II) into Pt(IV) via the following reaction

$$[PtCl_4]^{2-} + Cl^{\cdot} + H_2O \longrightarrow [PtCl_5(H_2O)]^{-}$$

Supplementary Note 2: force calculations

1) DLVO theory

The platinum oxide nanoparticles generated via photochemistry are subject to van der Waals and weak electrostatic interactions, which normally counteract with each other and can be described by DLVO theory (S2). The van der Waals interaction can be described using the following equation

$$U_v = -\frac{H_{PtO}}{6}\left(\frac{2r^2}{d(d+4r)} + \frac{2r^2}{(d+2r)^2} + In\frac{d(d+4r)}{(d+2r)^2}\right) \quad (1)$$

where H_{PtO} is the Hamaker constant of PtO, r is the radius of platinum oxide nanoparticles, d is the separation between two platinum oxide nanoparticles.

The electrostatic potential can be calculated with

$$U_{sc} = 2\pi\varepsilon r\psi_0^2[1 + \exp(-\frac{d}{L_d})] \quad (2)$$

where ε is the permittivity of the medium, $L_d$is the Debye length, $\psi_0$is the zeta potential of platinum oxide nanoparticles.

2) Optical dipole forces

The optical induced dipole forces between two platinum oxide nanoparticles (r=10 nm) at the focal plane of the Gaussian beam can be calculated using following formula (S3),

$$F = \int_S \mathbf{T}\cdot\mathbf{n}dS \quad (3)$$

Here **T** is defined as

$$T = \frac{1}{2}Re\left\{\varepsilon\mathbf{E}\bar{\mathbf{E}} + \mu\mathbf{H}\bar{\mathbf{H}} - \frac{1}{2}(\varepsilon\mathbf{E}\cdot\bar{\mathbf{E}} + \mu\mathbf{H}\cdot\bar{\mathbf{H}})\mathbf{I}\right\} \quad (4)$$

where **T** is Maxwell's stress tensor, S is the surface area of the platinum oxide nanoparticle, **n** is the unit vector normal to the surface and **I** stands the 3×3 identity matrix. We vary the separation between two platinum oxide nanoparticles and the optical forces along the x, y, z directions in space are plotted in Fig. S6.

The optical dipole potential can be calculated as

$$U_{opt} = -\int_{\infty}^{r_0}\mathbf{F}(\mathbf{r})\,dr \quad (5)$$

Thus, the total energy potential in X and Y directions are $U_x = U_v + U_{sc} + U_{opt}$ and $U_y = U_v + U_{sc}$, respectively (Fig. 2G).

Supplementary Note 3: photochemical deposition of metal sulfide

Metal sulfide (MS) particles are normally formed with the mixture of metal ions and S^{2-} ions. Here the S^{2-} ion is obtained from the sulfide source $Na_2S_2O_3$ which can be photochemically decomposed via the following reaction pathway (S4)

$$S_2O_3^{2-} + hv = S + SO_3^{2-}$$

$$2S_2O_3^{2-} + hv = S_4O_6^{2-} + 2e^{-}$$

$$M^{2+} + S + 2e^{-} = MS$$

Supplementary figures

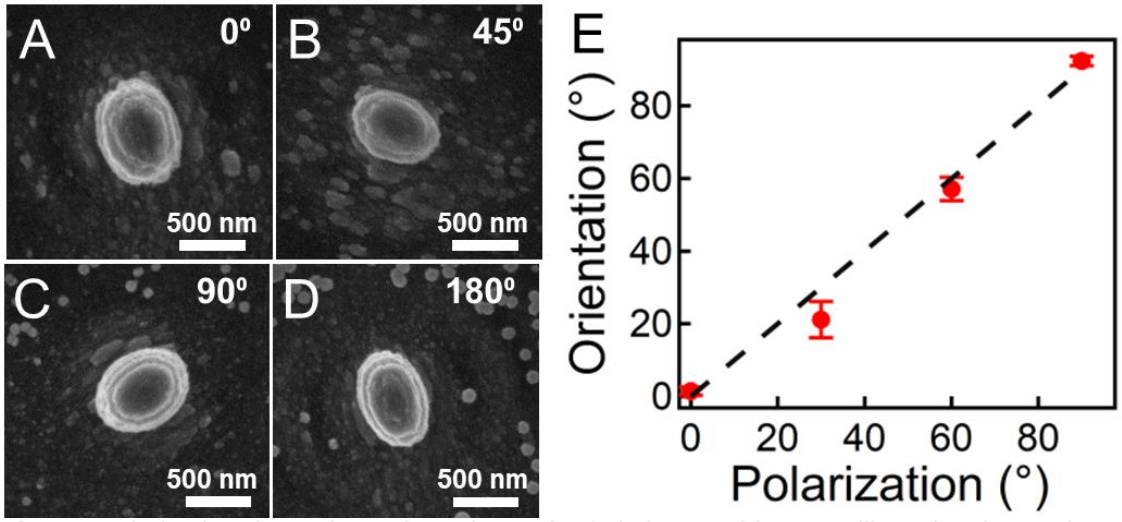

Fig. S1 Polarization-dependent oriented growth of platinum oxide nanopillars. (A-D) SEM images of elliptical nanopillars formed with different polarization directions. Concentration of the K_2PtCl_4 solution is 10 mM. Laser power: 3 mW, irradiation time: 10 s. (E) Change of the orientation with laser polarization direction. Error bars are the standard deviation of the orientation based on five elliptical nanopillars.

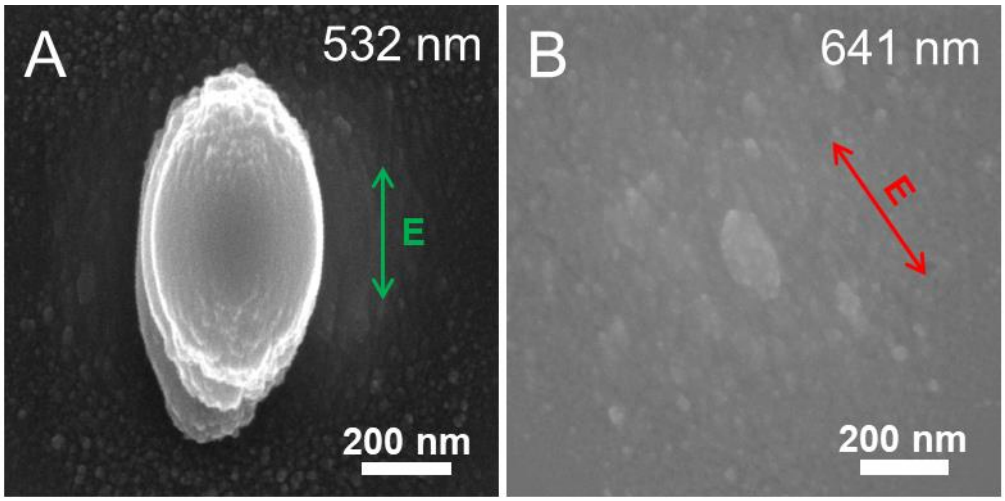

Fig. S2 Irradiation wavelength-dependent oriented growth of platinum oxide nanoparticles. Irradiation condition: (A) 532 nm CW laser at 3 mW for 15 s; (B) 641 nm CW laser at 4 mW for 80 s.

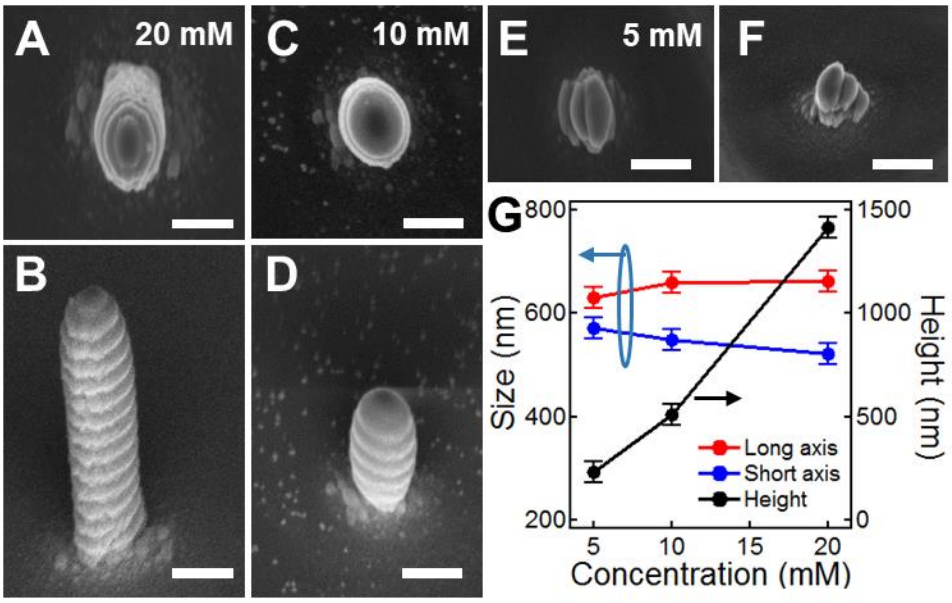

Fig. S3 Concentration-dependent oriented growth of platinum oxide nanopillars. Irradiation power: 3 mW, irradiation time: 10 s. Concentration of the K_2PtCl_4 solution: (A, B) 20 mM, (C, D) 10 mM, (E, F) 5 mM. (A, C, E) are top views and (B, D, F) are side views. Scale bars are 500 nm. (G) Change of the dimensions of nanopillars with the concentration of K_2PtCl_4.

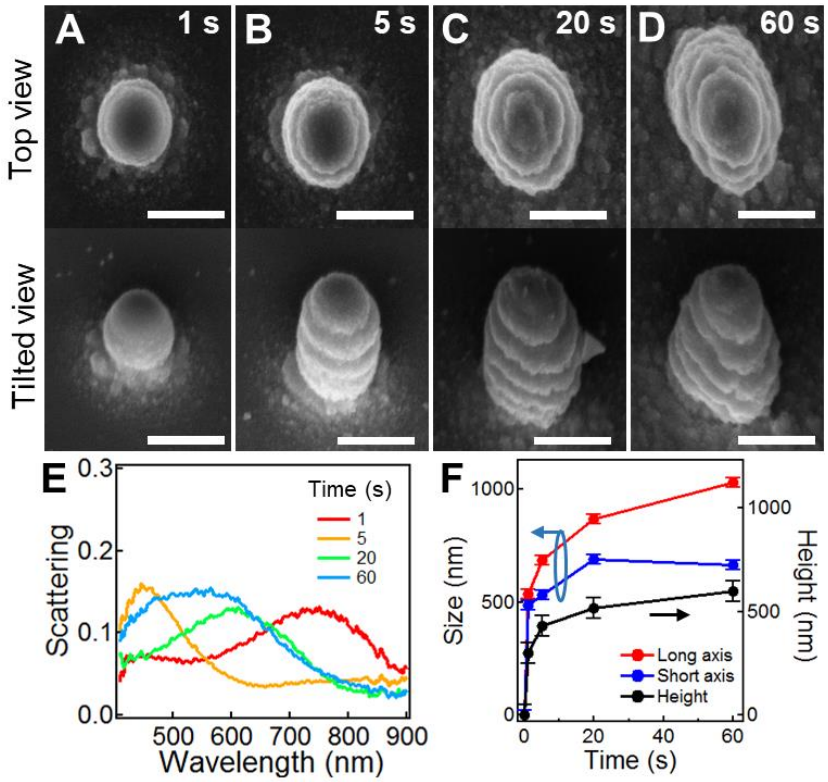

Fig. S4 Time-dependent oriented growth of platinum oxide nanopillars. (A-D) SEM images of nanopillars formed with different irradiation time. Concentration of K_2PtCl_4 solution is 10 mM. Irradiation power: 3 mW. (A) 1 s, (B) 5 s, (C) 20 s, (D) 60 s. Scale bars are 500 nm. (E) Scattering spectra of the platinum oxide nanopillars shown in (A-D). (F) Change of the sizes of the nanopillars with irradiation time.

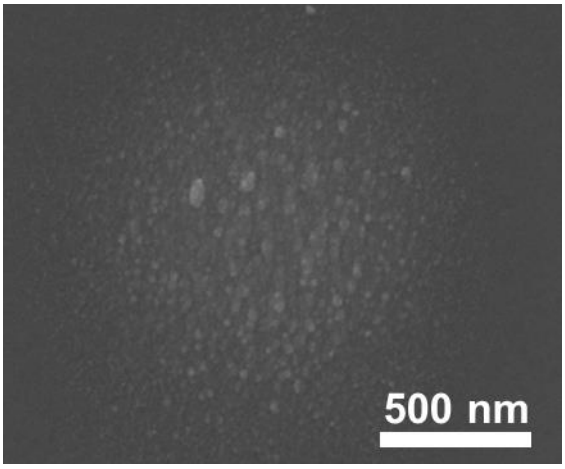

Fig. S5 SEM image of platinum oxide nanoparticles formed at initial stage of growth. Irradiation power: 1 mW, irradiation time: 1 s. Concentration of K_2PtCl_4 is 10 mM.

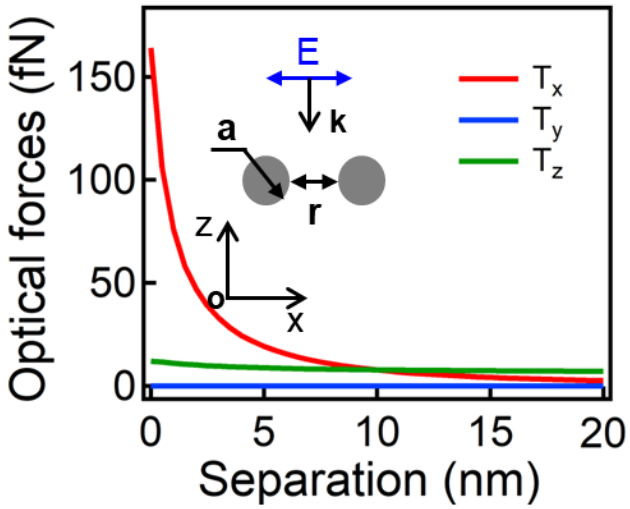

Fig. S6 Calculated optical forces along x, y, and z directions between two platinum oxide nanoparticles with different separations. Inset scheme denotes the axial system and the polarization direction of the incidence.

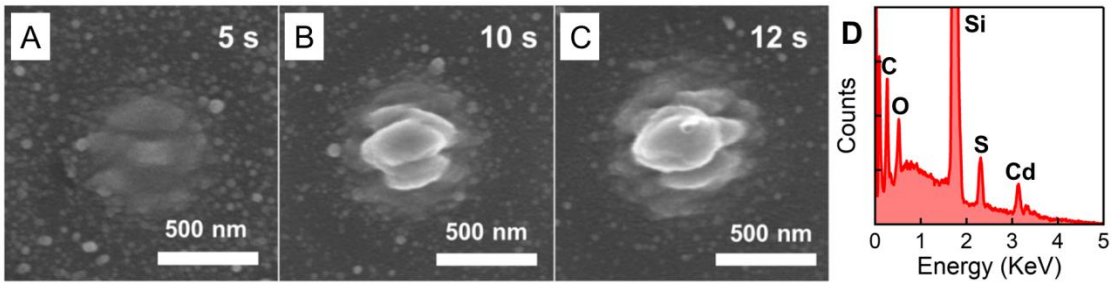

Fig. S7 Polarization-directed oriented growth of cadmium sulfide ellipsoids. (A-C) SEM image of CdS ellipsoids formed with different irradiation time and (B) its EDS.

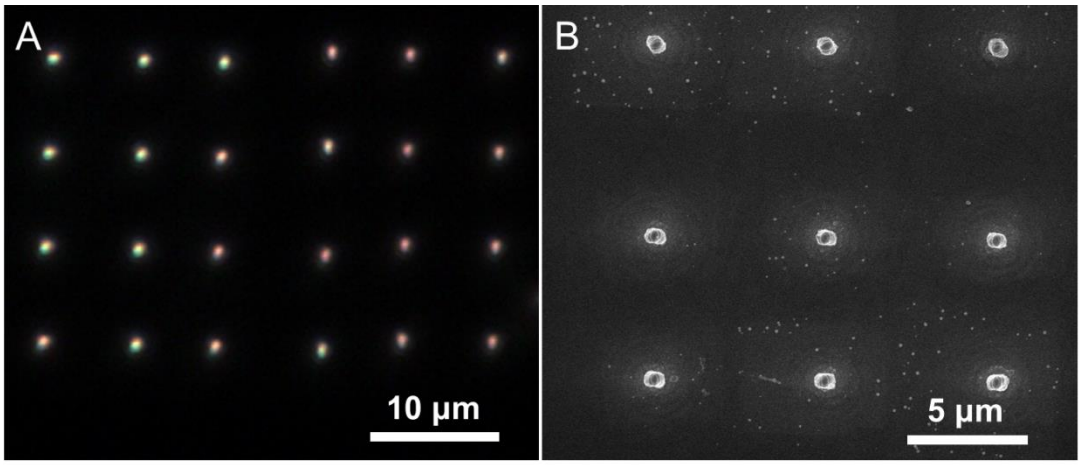

Fig. S8 Arrays of twisted platinum oxide micropillars fabricated by laser direct writing. (A) Dark field images, (B) SEM image.

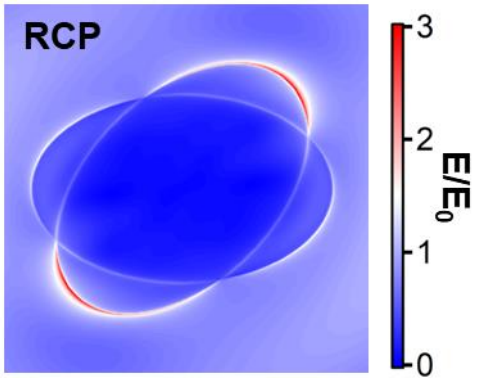

Fig. S9 Electric near field profile of twisted platinum oxide ellipsoids with incidence of RCP light (650 nm).

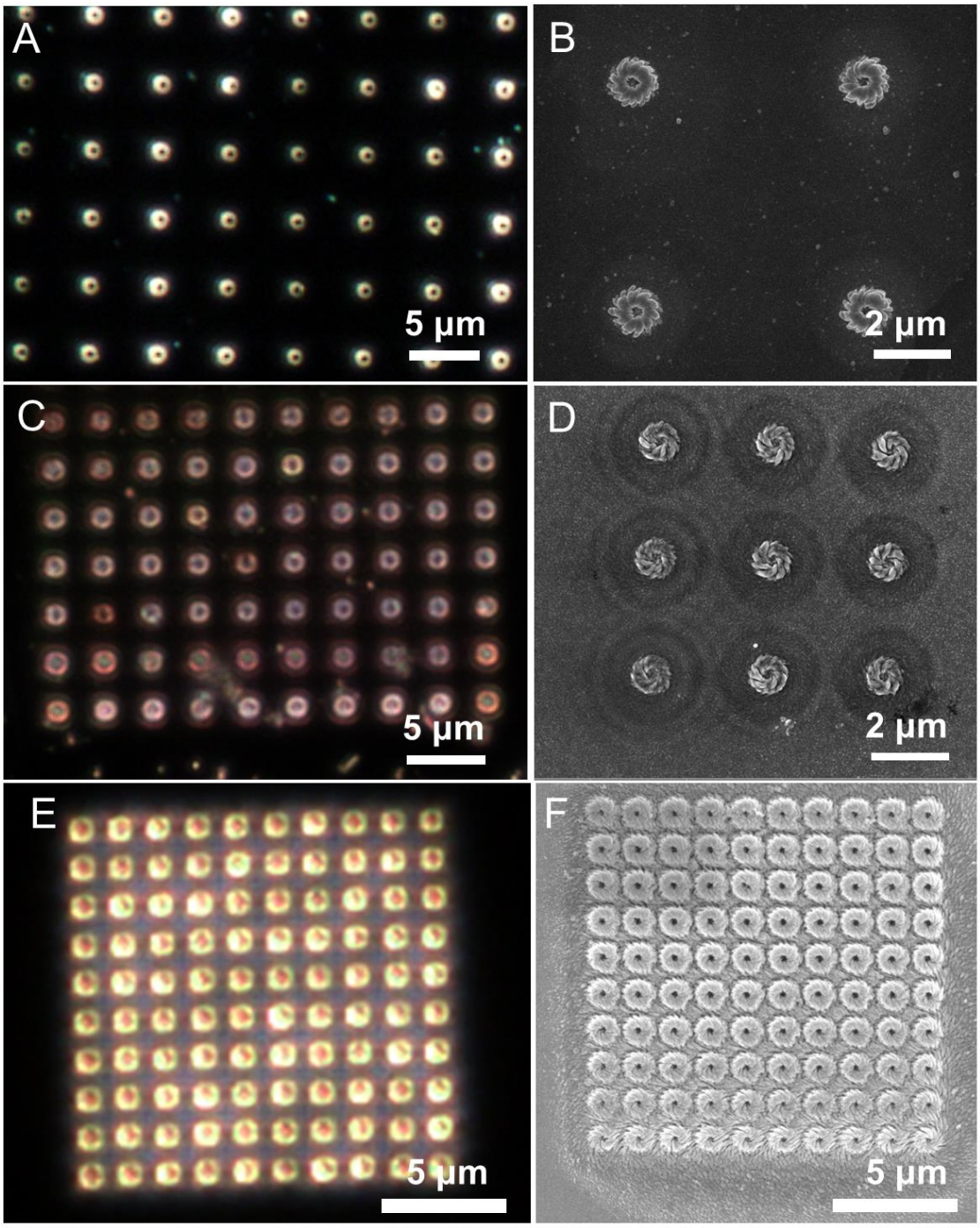

Fig. S10 Spiral nanostructures of (A, B) platinum oxide, (C, D) cadmium sulfide and (E, F) palladium oxide fabricated by laser direct writing with vector beams. (A, C, E) Dark field images. (B, D, F) SEM images.

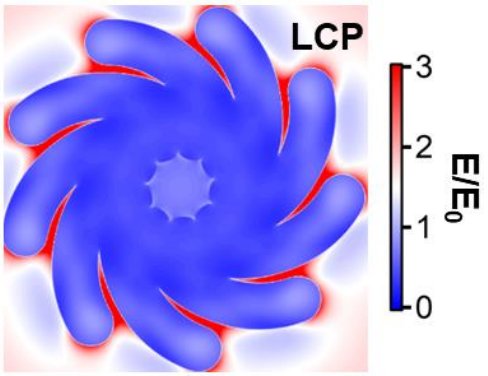

Fig. S11 Electric near field profile of left-handed spiral platinum oxide nanostructure with incidence of LCP light (510 nm).

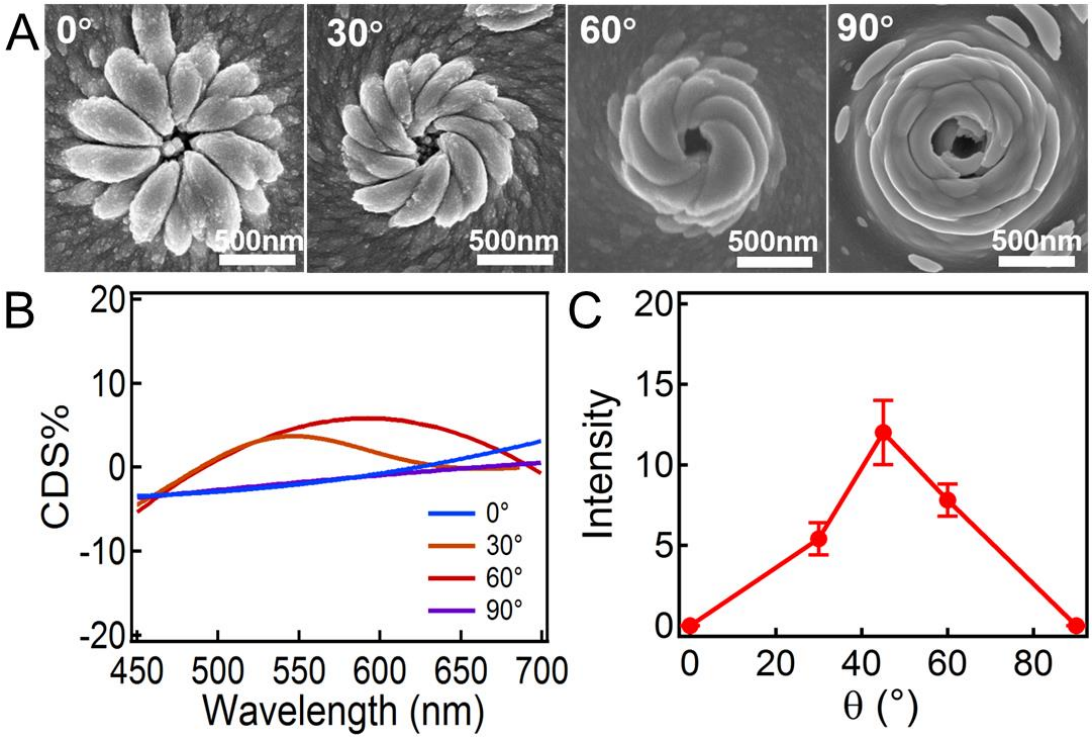

Fig. S12 Correlation of optical chirality with structural chirality. (A) SEM images of platinum oxide nanostructures with increasing alignment angle (θ) during the irradiation, (B) CDS spectra of platinum oxide nanostructures with different alignment angles. (C) Change of the CDS peak intensity with the alignment angle, showing the strongest chiroptic response with alignment angle of ~45°..

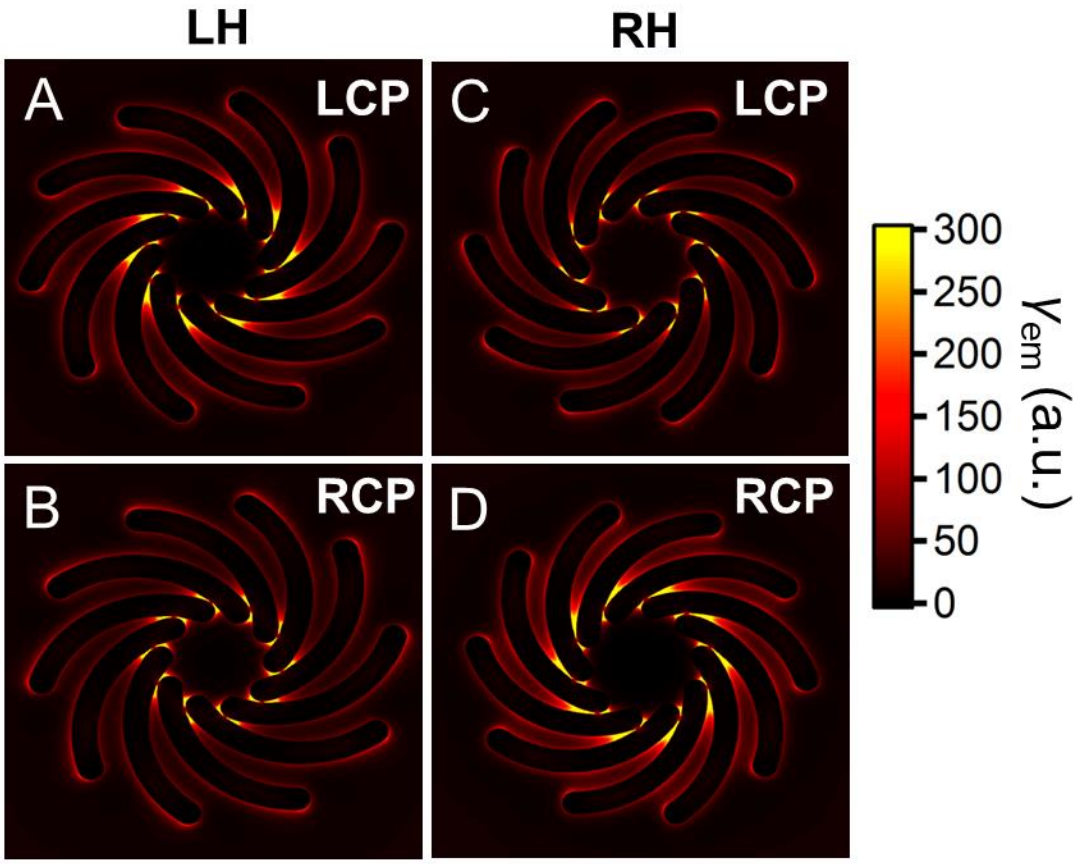

Fig. S13 Simulation of chiral emission rate of (A, B) LH and (C, D) RH cadmium sulfide nanostructures with (A, C) LCP and (B, D) RCP excitation.

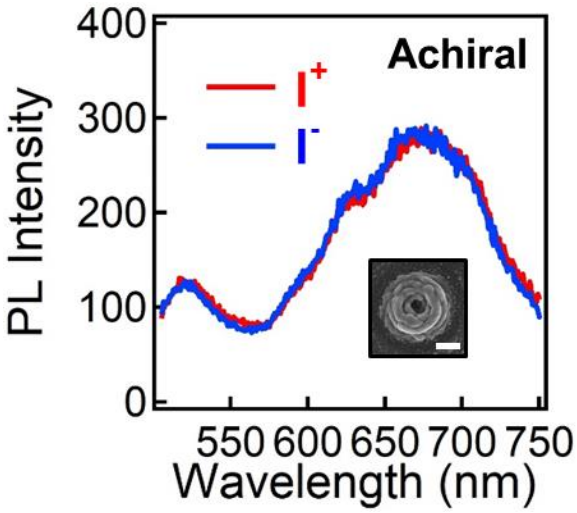

Fig. S14 PL spectra of achiral nanostructure of cadmium sulfide. I^+ and I^- denote the PL spectra excited with LCP and RCP beam respectively. Scale bar is 500 nm.

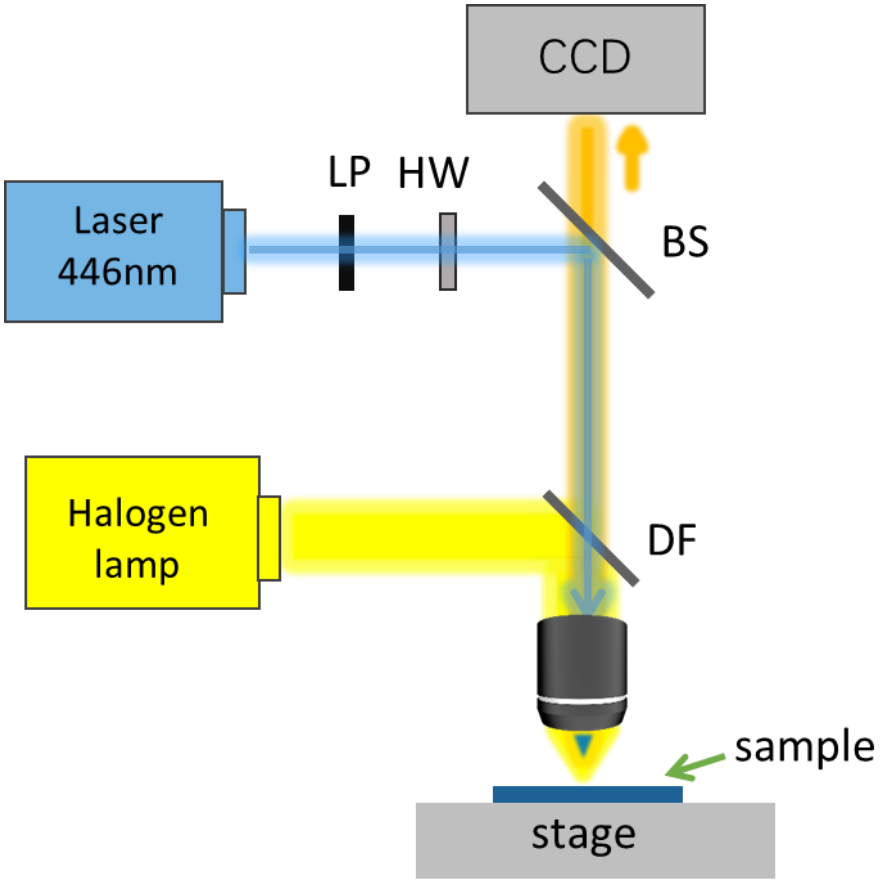

Fig. S15 Experimental setup of polarization-directed growth of twisted micropillars. LP: linear polarizer. HW: half-wave plate. BS: beam splitter. DF: dark field module.

Table S1. Comparison of different types of chiral nanostructures

Geometry	Method	g-factor	Wavelength (nm)	Reference
Chiral Ag nanoparticles	Glancing angle deposition	~10^{-3}	370	S5
Chiral Au nanoparticles	Chemical synthesis	~0.2-0.4	727, 622, 980	S6-S8
Helical Au nanoparticles	Self-assembly	~0.04-0.12	600-650	S9, S10
Plasmonic oligomers	Electron-beam lithography	~0.14	1100	S11
Au nanorod dimers	Self-assembly	~0.25	740	S12
HgS ellipsoids	Chemical synthesis	~0.0125	540	S13
CdTe twisted nanoribbons	Self-assembly	0.04	490	S14
PtO spiral structures	Laser direct writing	~0.2	450-750	This work

SI References

S1. I. V. Znakovskaya, Y. A. Sosedova, E. M. Glebov, V. P. Grivin, & V. F. Plyusnin Intermediates formed by laser flash photolysis of [ptcl6]2− in aqueous solutions. *Photochem. Photobiol. Sci* 4, 897-902 (2005).

S2. G. H. Findenegg J. N. Israelachvili: Intermolecular and surface forces (with applications to colloidal and biological systems). Academic press, london, orlando, san diego, new york, toronto, montreal, sydney, tokyo 1985. 296 seiten, preis: $ 65.00. *Berichte der Bunsengesellschaft für physikalische Chemie* 90, 1241-1242 (1986).

S3. Z. Li, M. Käll, & H. Xu Optical forces on interacting plasmonic nanoparticles in a focused gaussian beam. *Phys. Rev. B* 77, 085412 (2008).

S4. M. Ichimura, F. Goto, & E. Arai Photochemical deposition of cds from aqueous solutions. *J. Electrochem. Soc.* 146, 1028-1034 (1999).

S5. L. Yang, J. Liu, J. Deng, & Z. Huang Chiral nanoparticle-induced amplification in optical activity of molecules with chiral centers. *InfoMat* 2, 1216-1224 (2020).

S6. L. Xu*, et al.* Enantiomer-dependent immunological response to chiral nanoparticles. *Nature* 601, 366-373 (2022).

S7. H.-E. Lee*, et al.* Amino-acid- and peptide-directed synthesis of chiral plasmonic gold nanoparticles. *Nature* 556, 360-365 (2018).

S8. G. González-Rubio*, et al.* Micelle-directed chiral seeded growth on *anisotropic* gold nanocrystals. *Science* 368, 1472-1477 (2020).
S9. A. D. Merg*, et al.* Peptide-Directed Assembly of Single-Helical Gold Nanoparticle Superstructures Exhibiting Intense Chiroptical Activity. *J. Am. Chem. Soc.* 138, 13655-13663 (2016).
S10. J. Lu*, et al.* Enhanced optical asymmetry in supramolecular chiroplasmonic assemblies with long-range order. *Science* 371, 1368-1374 (2021).
S11. M. Hentschel, M. Schäferling, T. Weiss, N. Liu, & H. Giessen Three-Dimensional Chiral Plasmonic Oligomers. *Nano Lett.* 12, 2542-2547 (2012).
S12. K. W. Smith*, et al.* Chiral and Achiral Nanodumbbell Dimers: The Effect of Geometry on Plasmonic Properties. *ACS Nano* 10, 6180-6188 (2016).
S13. P.-p. Wang, S.-J. Yu, A. O. Govorov, & M. Ouyang Cooperative expression of atomic chirality in inorganic nanostructures. *Nat. Commun.* 8, 14312 (2017).